AIAA JOURNAL
Vol. 31, No. 10, October 1993

Skin-Friction Topology over a Surface Mounted Semi-Ellipsoidal Wing at Incidence

Timothy A. Johnson* and Virendra C. Patel†
Iowa Institute of Hydraulic Research, University of Iowa, Iowa City, Iowa 52242

Flow visualization methods have been used to study the skin-friction topology of a 12:6:1 semi-ellipsoid wing at incidence intersecting a plane wall. Results were obtained for incidences from 0 to 25 deg in 5 deg increments. Major changes in the topology demarcate divisions between general ranges designated as follows: symmetry, low, intermediate, and high incidences. As a function of incidence, the topological evolution is influenced by both three-dimensional pressure gradients and transition to turbulence. A slight twist in the experimental model suggests that the topology and associated separation modes (singular vs nonsingular) are highly sensitive to slight geometric asymmetries.

I. Introduction

FLOW separation around highly three-dimensional bodies intersecting walls is of great practical interest. Such configurations are found in one form or another on practically all hydro- and aerodynamic structures. In addition to the effects of lift, drag, and associated moments on the body itself, the complex wakes of these flows can influence the performance of downstream structures such as rudders and propellers. Unfortunately, the inherent unsteadiness and complexity of three-dimensional separated flows makes them, as of yet, beyond the reach of numerical methods. For this reason, experimental techniques remain particularly important in three-dimensional separated flow investigations.

In any continuous vector field there may exist points, designated singular points, at which the vector magnitude is zero. From our knowledge of two-dimensional flows, where separations are known to occur at points of zero skin-friction, these singular points are assumed to be intimately associated with separation in three-dimensional flows. A topological description of a vector field consists of a description of the types, locations, and connections among the singular points. There are two general types of surface singular points, nodes and saddles. Nodes are sources (attachment) or sinks (separation) of skin-friction vectors. Saddles occur at the intersection of two particular pairs of vectors; one pair of vectors leads in and collides head on with each other, and the second pair directs out laterally from the point of collision. Legendre[2] and Lighthill[3] proposed that flow separation be defined by the convergence of skin-friction vectors onto a particular line, the separatrix, tangent to the vector field and passing through a saddle point. Wang[4] expanded on this idea of separation by referring to this type of separation as "closed" and further introducing "open separation," so named due to their supposed downstream accessibilities to attached upstream flow. In the open case, separation occurs by convergence of vectors not onto a separatrix but onto a line involving only ordinary points. The consequence of this is that with no singular point associated with open separation, it will not appear in a solely topological flowfield description. The importance of differentiating between types of separations lies in the different effects these types are believed to have on aerodynamic and wake characteristics.

Many previous investigations have employed the topological features outlined above for describing separation patterns. Hunt et al.[6] present a study in which the flow patterns around cubes, cuboids, and axisymmetric humps are evaluated using topology to ensure kinematically correct flows. Tobak and Peake[7] comprehensively review the concept of flow topology, include a series of rules governing the occurrence of singular points on and around simply connected bodies, and provide examples of their application. Chapman[8] has even suggested a method of nomenclature and classification of three-dimensional flow separation based on the connections among singular points and including "cross-flow separation" to account for Wang's non-singular open separation.

In the present study, the separated flow over a surface mounted semi-ellipsoid is evaluated in terms of the topology of its skin-friction vector field. A slender ellipsoid was designed in an attempt to generate as interesting a flow as possible. The lack of sharp corners places no restriction on the separation location and allows three-dimenstional effects to influence the flow structure greatly. In addition, the mathematical simplicity of the model's geometry makes it ideal for possible computational studies.

As a first-order method, flow visualization has been used to detect the singular points on both the surface of the wing and the flat wall on which it is mounted. A slight geometric twist inadvertently built into the model provides for an interesting comparison, in terms of geometrical influence, with the results from a similar study using a symmetrical model. Reducing the separation pattern to a description of the singular points (type, location, and interconnections) greatly simplifies the separation description. In addition, changes in the topological structure with changes in flow parameter (angle of attack for this study) are made much easier to follow, allowing for a clearer understanding of the physical processes involved.

The skin-friction pattern has been visualized using a common surface oil flow method. Dye injection and smoke wire visualizations have also been used to determine the relationships between specific features of the surface shear-stress pattern and the surrounding flowfield. From the flow visualizations, wing and wall surface topologies have been constructed for angles of attack from 0 to 25 deg in 5 deg increments. It should be emphasized that only the surface topology is being studied here and that the dye and smoke methods were used solely to reinforce observations concerning the surface topology. Also, it is recognized that these methods are not without controversy and the accuracy of the results is often questioned. However, for preliminary investigation into complex topics the methods are very informative. Using rules governing the numbers and types of singular points, the topologies

Received Aug. 22, 1992; revision received Feb. 8, 1993; accepted for publication March 1, 1993. Copyright © 1993 by the American Institute of Aeronautics and Astronautics, Inc. All rights reserved.

*Graduate Research Assistant, Department of Mechanical Engineering. Student Member AIAA.

†UI Foundation Distinguished Professor of Mechanical Engineering and Research Scientist, Department of Mechanical Engineering. Associate Fellow AIAA.

have been checked for kinematic feasibility, as is required of a continuous vector field. Although these rules serve only as necessary, rather than sufficient conditions, they are nonetheless important criteria to be satisfied and should always be checked. The effect of the previously mentioned geometric twist on the separation has also been evaluated. The evolution of the separation is then traced as the angle of attack is varied, and the physical processes behind the topological changes are discussed.

II. Experimental Arrangement

Oil flow and smoke wire experiments were performed in the small 0.3 × 0.25 m open-end wind tunnel of the Iowa Institute of Hydraulic Research. Dye injection experiments were carried out in the Institute's 0.6-m square recirculating water flume.

The model geometry is depicted in Fig. 1. The wing is one-half of a 12:6:1 ellipsoid with a chord length of 0.205 m, and was mounted on the flat walls of the wind tunnel and water flume. For the wind tunnel experiments, the center of the wing was located three and one-half chord lengths from the contraction. In the water flume, for the dye injection, the test section was located approximately 5 m from the settling chamber. Although not illustrated in the figure, the wing had a slight geometric twist of approximately 2 deg over the last one third of its span. Because of this twist, the experiments were performed using two orientations. The twist effect could be changed from a slight increase in angle of attack of the tip, relative to the root, to a slight decrease by reversing the flow direction over the wing.

The oil flow method consisted of coating the surface of interest with an oil-based paint. When subjected to the wind tunnel flow, this paint produced streaks corresponding to the mean skin-friction lines. This procedure is described in detail

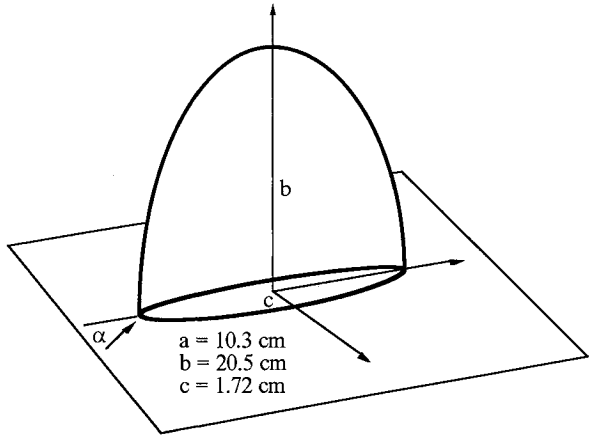

Fig. 1 Surface mounted semi-ellipsoidal wing.

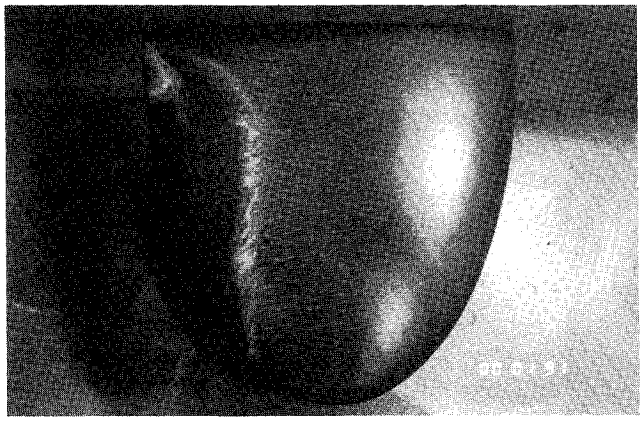

Fig. 2 Suction tip oil flow pattern: $\alpha = 0$ deg. Flow from left to right.

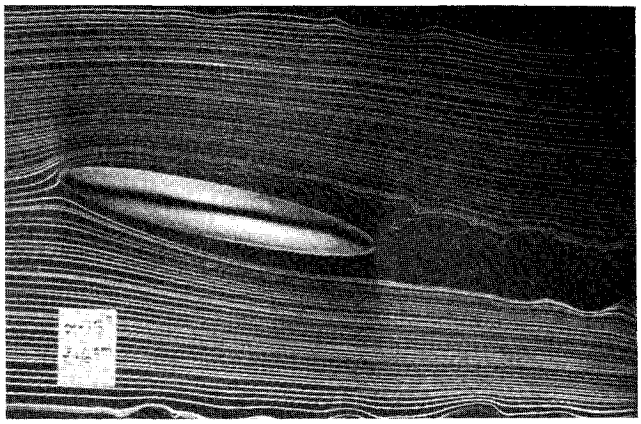

Fig. 3 Smoke wire result for $\alpha = 15$ deg.

by Maltby and Keating.[9] The composition of the paint used for this study was, by volume, 4 parts diesel oil, 1 part linseed oil, and 1 part titanium dioxide particles. The wind and wall surfaces were painted black to enhance the contrast with the white paint mixture. The paint was applied with an aerosol spray bottle. The experiments were run at a chord $Re = 2.5 \times 10^5$ corresponding to a freestream velocity of about 20 m/s. Pattern development was complete after 1–5 min. An example of the results generated by the oil flow method is shown in Fig. 2. This shows the wing surface skin-friction pattern at zero incidence.

A smoke wire was used to review flow characteristics of the surrounding flowfield. The apparatus consisted of a thin 0.1-mm diam stainless steel wire stretched across the test section of the wind tunnel a few centimeters upstream of the wing. After coating the wire with light mineral oil, a 1 amp current through the wire produced smoke lines, which were relatively evenly spaced along the length of the wire. Small springs were used to take up the slack that developed from the expansion of the heated wire. Photographs were taken in the flash of 0.8 μm strobes to provide frozen views of the streaklines. The freestream velocity was limited to 4 m/s to minimize disturbances from the wire. Thus, $Re = 5 \times 10^4$, or half an order of magnitude below that used with the oil flow method. However, since the attached flow of the wing surface was laminar in both cases, it is not likely that this disparity of Reynolds numbers makes limited comparisons between the experiments inappropriate, since flow patterns are often qualitatively similar on either side of transition. Figure 3 shows a representative result from the smoke wire method. The wing is at an angle of attack of 15 deg, and the smoke wire is located 6 cm spanwise from the wall.

Additional flowfield visualizations were performed using a water flume and injecting dye onto the wing surface and into the surrounding field. The dye consisted of potassium permanganate dissolved in water. To minimize excessive diffusion of the dye, $Re = 6 \times 10^4$, on the order of the smoke wire experiments.

III. Results and Discussion

It was discovered that the wing surface topology experiences two major changes, one between 5 deg and 15 deg, and the other between 15 deg and 20 deg. Based on these topological changes the results are divided into four general categories: the zero degree condition, low, intermediate, and high incidences. It is in terms of these categories that the skin-friction topology is presented for both suction and pressure sides of the wing surface as well as for the wall flow. In a few cases the complex geometry and the limitations of the experimental methods prohibit a clear evaluation of the real picture. In these cases, out of the many possible topologically correct flow patterns, the one with the lowest order (simplest) topology has been presented. The authors will attempt to make it clear when this presentation is the case.

A. Zero Degree Incidence

For the 0 deg condition, the wing's root was placed at a 0-deg angle of attack relative to the freestream. Naturally, however, the wing's twist means symmetry is not possible. With the root at 0 deg the twist produces two possible orientations of the wing: when the tip incidence is negative, the wing surface is in a "pressure tip" orientation; when the tip incidence is positive, the wing is in a "suction tip" orientation. Figure 2 shows the oil flow pattern at 0 deg for the suction tip orientation, with flow from left to right. The bright areas in the figure on the upstream half of the wing are simply reflections of the light source. The oil pattern for the pressure tip orientation is not shown, since it differs only very slightly from Fig. 2. This difference is illustrated, however, in the sketches discussed at follows. A sketch of the skin-friction topology for 0 deg is shown in Fig. 4. Here, the pressure tip orientation is on the left, the suction tip in the center, the trailing edge (labeled T.E.) on the right, and the wall flow pattern on the bottom.

Figure 4 shows the flow attaching to the wing at nole $N1$, which is shown split between both the pressure and suction tip sides. The flow remains attached and roughly parallel to the freestream direction over the first 75 percent of both of the wings surfaces. As about the three-fourths chord location and on both sides of the wing, the flow separates along lines essentially perpendicular to the freestream. In Fig. 2 this line is the heavy line of oil accumulation on the right side of the wing. As the separation line approaches the root, it turns abruptly downstream toward the trailing edge. Located on this primary separation line and about one-third span from the wall are saddle points denoted in Fig. 4 as $S1_P$ and $S1_S$, for pressure and suction sides, respectively. At the downstream end of the separation in Fig. 2 there is an accumulation of oil in the shape of a disfigured circle. This accumulation of oil indicates the presence of spiral nodes of separation $N2_P$ and $N2_S$. These nodes are presumably the footprints of where the separating streamsurfaces roll up into free vortices. A second spot of oil accumulation, again present on both sides of the wing and located between the wall and the $N2$'s, indicates a second node $N3_P$ and $N3_S$ for each side. These $N3$ nodes are associated with the trailing edge nodes present on the wall pattern in the bottom of Fig. 4 and discussed later. The extended region of attached flow located between nodes $N2_{S,P}$ and $N3_{S,P}$ is likely a result of turbulence in the boundary layer. The mixing of the turbulent boundary layer serves to delay separation along the wing surface adjacent to the wall.

Because of the separated flow over the trailing edge, the oil pattern is underdeveloped and the skin-friction vectors are not clearly distinguishable. In the next section, on the low incidence case, the stronger, more deliberate, separated flow shows much clearer results. There, use will be made of more detailed experimental evidence to substantiate the topological interpretation. For now, to complete the wing surface topology, use must be made of the known flow directions immediately surrounding the underdeveloped region. This process implicitly involves the use of the Poincaré-Bendixson Index Theorem, a thorough discussion of which is given in Hunt et al.[6]

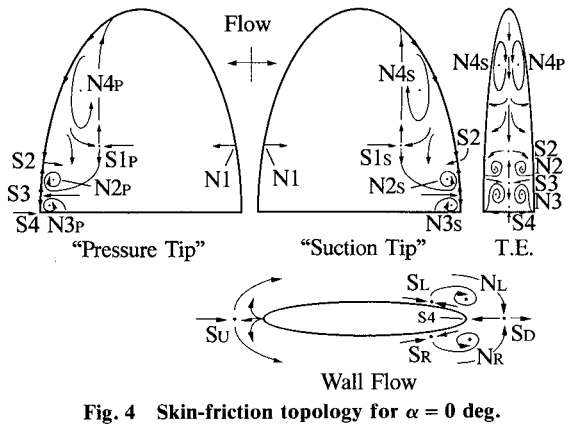

Fig. 4 Skin-friction topology for $\alpha = 0$ deg.

Dye injection showed that the flow over the tip moved along the trailing edge toward the root. The skin-friction vectors on the trailing edge in Fig. 4 have been drawn accordingly. However, between the symmetric nodes $N2_p$ and $N2_s$, flow is necessarily induced away from the root. The intersection point of these two opposing directions produces a saddle $S2$. Between the node pairs $N2$ and $N3$ flow is again induced in opposite directions; up between the $N2$'s and down between the $N3$'s. This results in the need for $S3$. Likewise, at the base of the wing, downward flow from $N3_P$ and $N3_S$ collides with reverse flow on the wall to produce a fourth saddle $S4$. Lastly, there are two regions, each bordered by the trailing edge, where flow is down; the separation line, where flow is up; and the separatrix approaching $S1$ ($_S$ or $_P$) from downstream. The consistent rotational direction of the vectors surrounding these regions requires the presence of nodes $N4_P$ and $N4_S$. Naturally, this method of determining the presence of singular points is somewhat gross. The best it can do is determine the net effect of what may be multiple singular points within the region of interest. Indeed, one can draw an infinite number of possible topologies to fit the observed flow directions. For this reason the topology on the trailing edge in Fig. 4 is left as the simplest possible, first-order structure. Since it is known that saddle-saddle connections are unstable,[1] the line of $S2$-$S3$-$S4$ is certainly undesirable. However, the difficult geometry coupled with the separated flow of the trailing edge makes an exact determination of the topological structure very difficult.

The flow at the tip is another region where the topology is difficult to resolve. It is not certain how the separation lines behave at the tip. It is known that because of a slight asymmetry, the two separation lines (pressure and suction) do not meet. The most likely possibility is that each line bends into an $N4$ node, making these nodes of separation. Other possibilities exist, where multiple node-saddle combinations sit at the end of the separation line, but with no evidence to support this, the previous interpretation remains.

The wall pattern, shown at the bottom of Fig. 4, is relatively straightforward. An upstream saddle S_U occurs at the intersection of the upstream flow and reverse flow caused by the obstruction. As shown by Hung et al.[5] this saddle could be a saddle of either separation or attachment. To resolve this ambiguity the flowfield would have to be known. Toward the trailing edge the flow separates from both sides of the wing base at saddles S_L and S_R. The flow closes again just downstream of the trailing edge at S_D and encompasses nodes N_L and N_R. This pattern looks similar to flowfield separations around two-dimensional geometries. Notice that it is the reverse flow from S_D that approaches the root of the wing and intersects with the downward flow between $N3_P$ and $N3_S$ resulting in $S4$.

In light of the conjecturing required to complete the wing surface skin-friction pattern, a procedure is desired to help ensure that the kinematics of the vector field are not violated. To this end, a rule from Hunt et al.[6] and included in Tobak and Peake's[7] list of singular point rules can be applied. It states that for a simply connected body in conjunction with a plane wall, there must be an equal number of nodes and saddles on the wing and wall surfaces combined. A tally of the nodes and saddles present on these surfaces is as follows:

Nodes: $N1$, $N2_P$, $N2_S$, $N3_P$, $N3_S$, $N4_P$, $N4_S$, N_L, $N_R = 9$

Saddles: $S1_P$, $S1_S$, $S2$, $S3$, $S4$, S_U, S_L, S_R, $S_D = 9$

Therefore, on the pressure, suction, and wall surfaces there are nine nodes and nine saddles. This is consistent with the topological rule indicating that the pattern is kinematically feasible. Note that this does not ensure correctness of the pattern, only that the kinematics are not violated. The rule

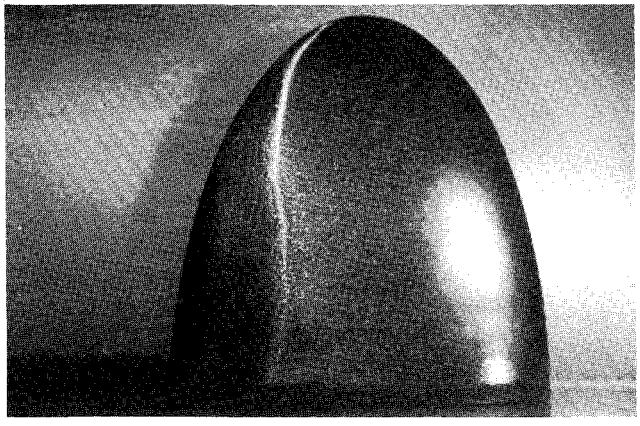

Fig. 5 Pressure side oil flow pattern for $\alpha = 5$ deg. Flow from right to left.

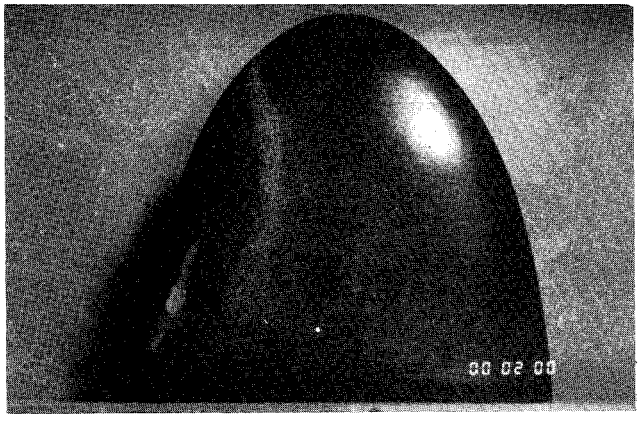

Fig. 6 Suction side oil flow pattern for $\alpha = 5$ deg. Flow from right to left.

allows for the addition or subtraction of singular points as long as it is done in node-saddle pairs, hence the possibility for an infinite number of conjecturable patterns.

As Fig. 4 indicates, the skin-friction pattern at 0 deg is topologically symmetrical with respect to the pressure and suction tip sides. In other words, for each node or saddle present on the suction side, an analogous node or saddle is present on the pressure side. However, as illustrated, a slight asymmetry is present in terms of geometrical location. On the suction side, the separation line remains perpendicular to the wall as it extends along the wing in the spanwise direction. It eventually terminates off the outer portion of the trailing edge. On the pressure side, however, as the separation line approaches the tip, it turns upstream and terminates very close to the tip. The role of the wing's twist in this asymmetry can be explained when considering the results at low incidence.

B. Low Incidence

Low incidence is taken as the range of angles of attack above zero and below the first major topological change somewhere around 10 deg. Results for the low incidence range were obtained at 5 deg. Figure 5 shows the oil pattern on the pressure side, and Fig. 6 shows the suction side. At this and all other nonzero incidences the twist was found to have no observable influence, and so only one orientation was used, with flow from right to left in all cases. The topology for the low incidence case is shown in Fig. 7, again with the pressure side on the left, suction side in the center, trailing edge on the right, and the wall flow on the bottom. Keep in mind that although the photographs all show the flow from right to left, the suction side topology is sketched with flow from left to right.

On the wall, as shown in Fig. 7, the upstream and downstream saddles S_U and S_D are still present but at the trailing edge, only one node N_R and one saddle S_R remain. The pressure gradient at the root on the pressure side has apparently become favorable enough to keep the boundary layer from separating at the wing-wall junction. Because of this, the node-saddle pair N_L-S_L on the wall in Fig. 4 has disappeared in Fig. 7. Incidentally, the node that was $N3_P$ on the wing surface of Fig. 4 has also disappeared. This result reinforces the implication of an intimate association between the wing surface nodes $N3_P$ and $N3_S$ and the wall surface nodes N_L and N_R in Fig. 4.

Aside from the disappearance of node $N3_P$ at the trailing edge root, the low incidence pressure side is much the same as the pressure tip side at 0 deg. A separation line, indicated by the accumulation of oil on the left side of the wing in Fig. 5, is located at about 75% chord and turns slightly upstream as it approaches the tip. In Fig. 7, the flow is shown attaching on the pressure side at $N1$ and moving downstream to this separation line at $S1_P$. Whereas the oil pattern just downstream of the separation line for the zero incidence case was underdeveloped, for the low incidence case it is quite clear and shown in Fig. 8. The divergence of the flow at the saddle point $S1_P$ is plainly obvious, as is the rotation about node $N4_P$.

On the suction side another separation line occurs at essentially the same 75% chord location, but rolls up at node $N2_S$ corresponding to the heavy spot of oil on the left side of the wing in Fig. 6. As the separation approaches the tip it exhibits no upstream turn, terminating off the distal trailing edge. Also, as shown in the picture and illustrated in the sketch, there is no longer a saddle point on the separation line and no node $N4$. The reason for this change in topology can be found by considering the spanwise pressure gradient. On the suction side, the effect of the variable chord length is to generate a

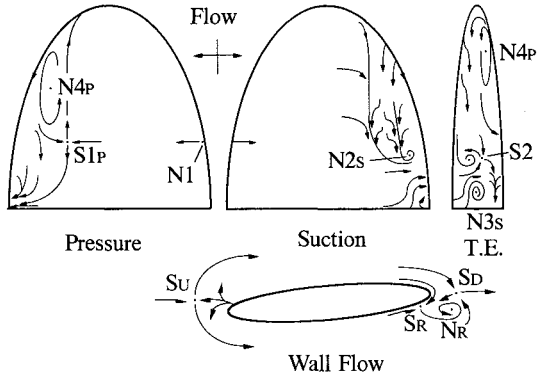

Fig. 7 Skin-friction topology for $\alpha = 5$ deg.

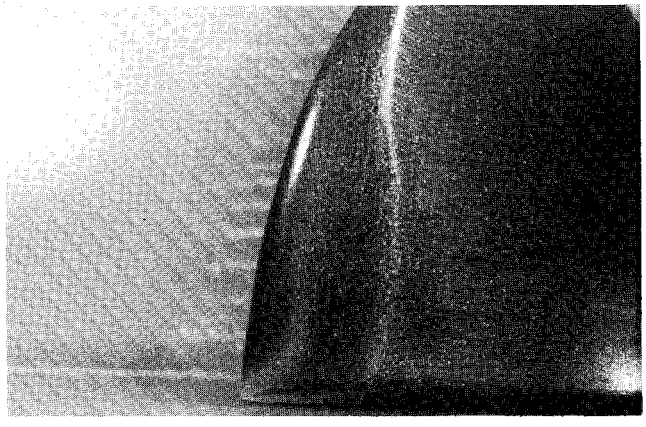

Fig. 8 Pressure side oil flow pattern downstream of separation for $\alpha = 5$ deg. Flow from right to left.

spanwise pressure gradient that pushes flow from the tip toward the root. With all the flow turned toward the root, the saddle point is eliminated, and since the $N4$ nodes can exist only with flow on the separation line toward the tip, these nodes also disappear.

Although not obvious in Fig. 5, the opposite effect should take place on the pressure side. In this case, the spanwise pressure gradient turns the flow toward the tip, and the saddle point moves toward the root.

At the tip the behavior of the pressure side separation line is assumed to be similar to that at 0 deg. As a first approximation, the line is simply assumed to lead directly into node $N4_P$ after turning sharply downstream at the tip. On the suction side the separation is open and no assumption needs to be made.

The trailing edge pattern of the wing is shown on the right side of Fig. 7. Two additional singular points are present in this view, $S2$ and $N3_S$. Figure 9 shows a close-up of the suction side trailing edge corner. On the wing surface, near the root, the oil lines can be seen turning away from the wall. This behavior is also shown at the analogous location in the sketch of Fig. 7. This implies the existence of node $N3_S$ at the trailing edge. The saddle point $S2$ is a necessary feature to account for the intersection of flow moving up around $N2_S$ and flow moving down along the trailing edge. Once again, $S2$ represents a first-order approximation of the topology at the trailing edge since the exact structure could not be resolved with much detail.

The kinematics of the flow topology can be ensured with a quick count of the singular points.

Nodes: $N1, N2_S, N3_S, N4_P, N_R = 5$

Saddles: $S1_P, S2, S_U, S_R, S_D = 5$

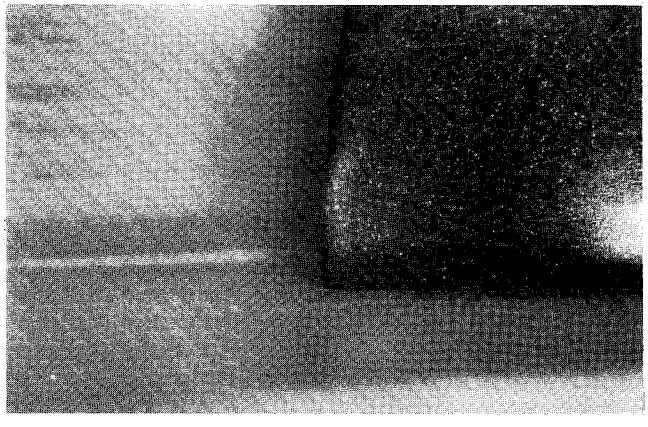

Fig. 9 Close-up of suction side trailing edge for $\alpha = 5$ deg. Flow from right to left.

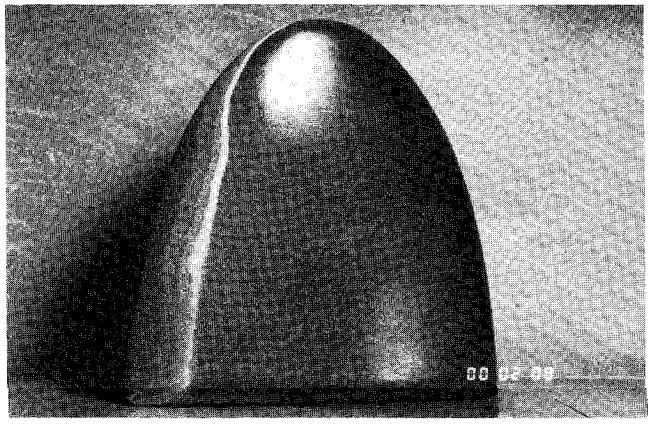

Fig. 10 Pressure side oil flow pattern for $\alpha = 15$ deg. Flow from right to left.

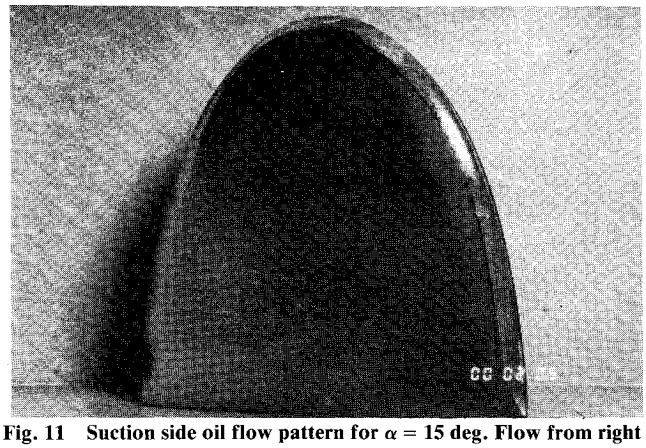

Fig. 11 Suction side oil flow pattern for $\alpha = 15$ deg. Flow from right to left.

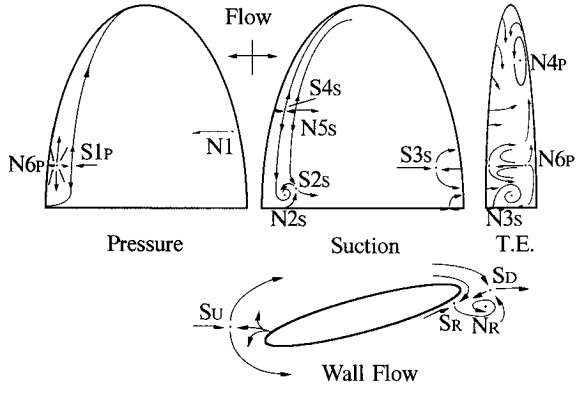

Fig. 12 Skin-friction topology for $\alpha = 15$ deg.

Now, with the same trend just seen in the discussion of 5 deg, the slight asymmetry of the separation line near the tip that was observed at 0 deg can be explained. When the twist produces a pressure gradient that pushes flow toward the tip, as on the pressure tip side, the separation line bends with a tendency to separate parallel to the edge of the wing. Therefore, on the pressure tip side the separation line extends along the edge to the tip. On the suction tip side the opposite effect, a pressure gradient pushing flow toward the root, holds the separation back on the trailing edge.

It should be pointed out that in a more extensive study by Johnson,[11] the model was replaced with a symmetrical wing. This replacement produced a pattern geometrically as well as topologically symmetrical at the tip, with nonsingular separations on both sides of the wing. In other words, the saddle points $S1_P$ and $S1_S$ of Fig. 4 and their associated nodes $N4_p$ and $N4_s$ did not appear, and both separation lines were open. The relatively slight asymmetry of the twist illustrates how sensitive the flow structure is with regard to small boundary condition perturbations.

C. Intermediate Incidence

Somewhere around 10 deg a major change in the topology occurs. Angles of attack above 10 deg and below 20 deg (the second major change) fall in the intermediate incidence range. Characteristic results were obtained at 15 deg and are shown for pressure and suction sides in Figs. 10 and 11, respectively. The topology sketches for this range are shown in Fig. 12.

On the pressure side, Figs. 10 and 12 show that the separation line has moved downstream relative to that of the low incidence case. The saddle point $S1_P$ has moved toward the root consistent with the spanwise pressure gradient effect that

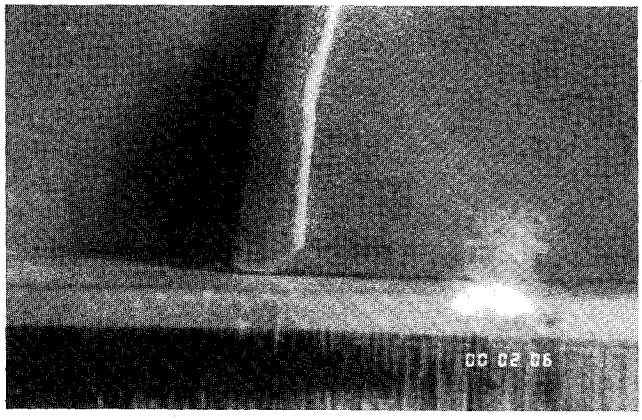

Fig. 13 Close-up of pressure side trailing edge for $\alpha = 15$ deg. Flow from right to left.

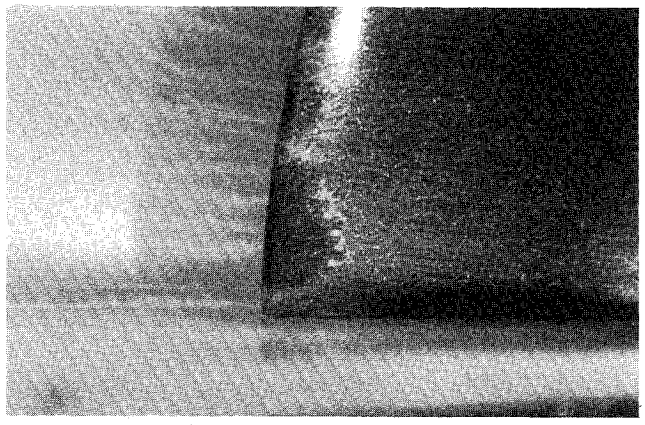

Fig. 14 Close-up of suction side trailing edge for $\alpha = 15$ deg. Flow from right to left.

pushes flow toward the tip on the pressure side. Node $N4_P$ is still present due to the opposing directions of flow toward the root on the trailing edge and toward the tip on the separation line. It is depicted on the trailing edge at the right in Fig. 12 rather than on the pressure side. A new node $N6_P$ has appeared at the trailing edge of the pressure side. A close-up view of this node is shown in Fig. 13 where the oil lines can be seen spreading out from one point just downstream (to the left) of the separation. Its nonfocus, or nonspiral, appearance characterizes it as a node of attachment rather than separation.

The suction side of the wing has experienced the most dramatic changes. This result is evident when comparing Figs. 11 and 12. Because of the increase in angle of attack, the flow no longer remains attached at the leading edge. Instead, it separates along the line in Fig. 12 containing saddle point $S4_S$. This line extends from the tip nearly to the root, where it terminates within the boundary layer and rolls up into node $N2_S$. Figure 3 shows a smoke wire picture of the flow around the wing at 15 deg. It can be seen that after the flow separates from the leading edge it becomes turbulent. As was pointed out above, the smoke wire experiments were performed at a Reynolds number one-fifth of that for the surface oil visualizations. For the higher Reynolds number, the turbulent transition would be expected to take place on the order of one-fifth the distance. This transition to turbulence causes the flow to reattach to the wing surface along the line of attachment identified in Fig. 12 by node $N5_S$. The effects of having turbulent flow over the remaining portion of the wing are the delay and constriction of the separation zone. Previously, at low incidence (Fig. 7), the separation took place at roughly 75% chord, spanning over two-thirds of the wing. Now at intermediate incidence, the suction side turbulent flow pushes the separation line back toward the trailing edge and bends the outer length over to form the small scallop-shaped separation containing two lobes of reversed flow at saddle $S3_S$. An enlarged view of this phenomenon is shown in Fig. 14. It is this reversed flow that originates from reattachment node $N6_P$ on the pressure side. Between the separation line of $S3_S$ and the root, a node $N3_S$ is believed to occur. Although this cannot actually be seen in the photographs, its existence is based on the presence of node N_R on the wall as well as results from additional experiments using a larger model.[11]

The details of the separation line at the tip are not known. Again, multiple saddle-node combinations would satisfy the kinematics, but have been left off in favor of simplicity.

Compared with the results at low incidence (Fig. 7), the wall flow of Fig. 12 has not changed topologically. Both the upstream and downstream saddles S_U and S_D are still present, and again, only one node N_R and one additional saddle point S_R are present.

The singular point tally gives:

Nodes: $N1, N2_S, N3_S, N4_P, N5_S, N6_P, N_R = 7$

Saddles: $S1_P, S2_S, S3_S, S4_S, S_U, S_R, S_D = 7$

again satisfying the kinematic requirements.

D. High Incidence

The onset of the high incidence regime is characterized by the second major shift in topological structure occurring at approximately 20 deg. The results were obtained at 25 deg and are shown in Fig. 15 with the flow from right to left. Only the suction side oil pattern is presented since the high incidence pressure side pattern remained virtually unchanged from the intermediate incidence case.

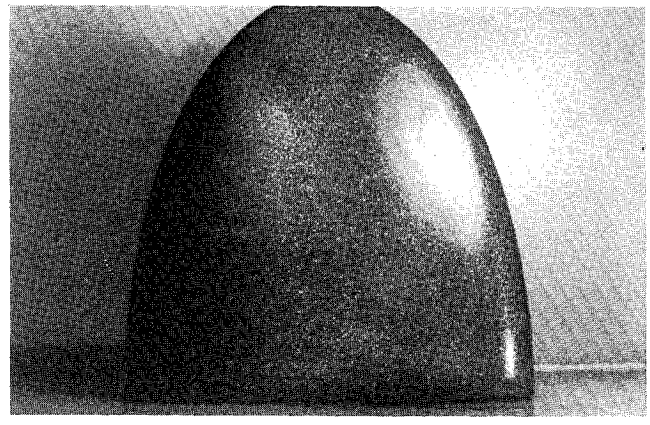

Fig. 15 Suction side oil flow pattern for $\alpha = 25$ deg. Flow from right to left.

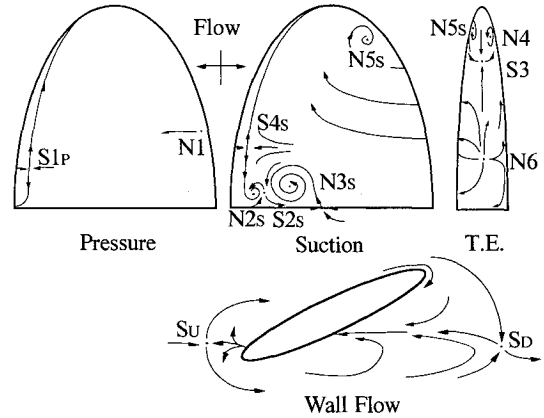

Fig. 16 Skin-friction topology for $\alpha = 25$ deg.

The pressure side pattern is sketched in Fig. 16 and is essentially the same as that of Fig. 12. The separation line is pushed farther downstream, and the saddle point moves spanwise slightly toward the wall, again consistent with the increasing spanwise pressure gradient. Downstream of the separation, no singular points are shown in the pressure side sketch, since they have moved all the way to the trailing edge.

At the trailing edge, in Fig. 16, the familiar node $N4$ shows up. Once again, $N4$ is a first-order approximation required due to the local flow directions at the separation line and the trailing edge. The node $N6$ in the sketch is the same reattachment node as $N6_P$, which fed the small separated region at $S3_S$ in Fig. 12.

On the suction side, with the angle of attack increased to 25 deg, the flow separating off the leading edge becomes turbulent, but unlike the intermediate incidence case, is unable to reattach to the surface. Therefore, the entire suction side is separated, reversed flow. This massive separation allows the previously small and constricted scallop-shaped separation at intermediate incidence to grow and engulf the suction side completely. This result occurs when saddle $S3_S$ from Fig. 12 moves upstream to the leading edge and merges and disappears with node $N5_S$, also of Fig. 12. The upper and lower lobes of reverse flow of the $S3_S$ separation expand in the process to become nodes $N3_S$ and $N5_S$ in Fig. 16. The numbering method here should not be confused; the node $N5_S$ of Fig. 16 is a new node of separation at high incidence, and the node $N5_S$ of Fig. 12 is the reattachment of the separated flow to the wing surface at intermediate incidence. The source of the reversed flow is still a node of attachment $N6$ at the trailing edge and analogous to $N6_P$ of Fig. 12. The node-saddle combination of $N2_S$ and $S2_S$ was difficult to resolve in photographs, but its presence could be seen by close examination during the actual experiment.

The separation line containing $S4_S$ on the suction side extends all the way to the tip of the wing and connects with the pressure side separation line containing $S1_P$. This behavior makes sense when one considers the situation as the angle of attack approaches 90 deg. At 90 deg the pressure side separation line will have moved all the way downstream to what was the trailing edge, and the suction side separation will be located on what was the leading edge. At 90 deg, however, with no distinction between trailing and leading edge, the wing is simply a bluff body with a continuous separation line along the perimeter of the plan surface area. In fact, by 25 deg the separation line is already continuous from pressure to suction side, and the separation is truly a region of closed separation.

The wall flow has changed somewhat from intermediate to high incidence. A picture of the flow pattern is shown in Fig. 17. Both S_U and S_D clearly remain. However, the trailing edge node that was N_R in Fig. 12 has apparently merged and disappeared with the saddle that was S_R. This interpretation is made with the aid of LDV measurements taken around the same geometry by Parthasarathy et al.[10] Interestingly, there is also no node on the wing suction surface analogous to the trailing edge nodes $N3_S$ of previous incidences. This is further evidence that the nodes $N3_S$ on the wing and N_R on the wall are a result of a single flowfield feature. It should be pointed out that dye and smoke visualizations reveal that all of the reverse flow indicated by Fig. 17 is constrained to a fairly thin region near the wall, on the order of the boundary-layer thickness.

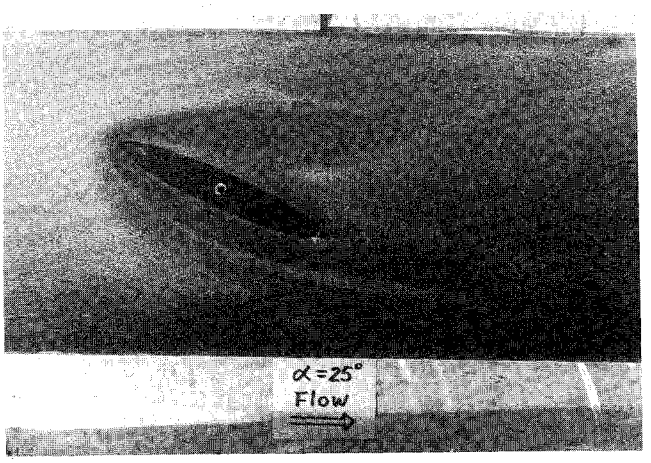

Fig. 17 Wall flow oil pattern for $\alpha = 25$ deg. Flow from right to left.

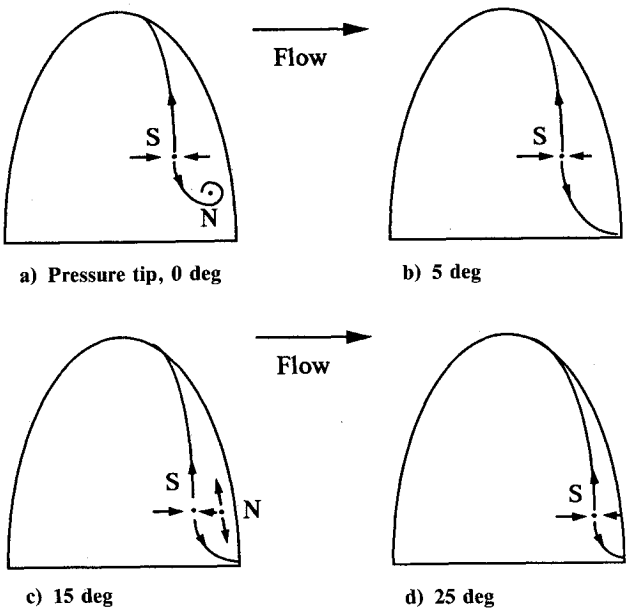

Fig. 18 Evolution of pressure side topology.

A tally of the high incidence singular points also shows the topology, with seven nodes and seven saddles, to agree with the topological rule.

Nodes: $N1, N2_S, N3_S, N4_P, N5_S, N6, N_R = 7$

Saddles: $S1_P, S2_S, S3_S, S4_S, S_U, S_R, S_D = 7$

E. Topological Evolution

From the previous discussion it was seen that the topology of skin-friction vectors on the wing goes through quite drastic changes as the angle of attack increases. These changes are influenced by the nature of the flow as well as the three-dimensional geometry of the wing. In this section the evolution of the topology is traced in terms of the gross features, and the physics governing the evolution processes is discussed.

A skeletal representation of the pressure side topology at each angle of attack is shown in Fig. 18. The flow is from left to right, and only the basic features are indicated, with nodes represented simply by N and saddles by S. At 0 deg (Fig. 18a) the orientation shown is the pressure tip, where the small geometric twist gives the tip a small positive incidence. The basic topology consists of a singular separation line at about 75% chord, which rolls up into a node near the base. At the tip the separation line turns slightly upstream due to the spanwise pressure gradient generated by the pressure tip. At 5 deg, shown in Fig. 18b, the pattern remains very similar, with only the node disappearing from the base of the wing due to the increased favorable pressure gradient around the trailing edge. At the tip the separation line turns slightly upstream, again due to the spanwise pressure gradient that develops on the pressure side. In Figs. 18c and 18d, the patterns for intermediate and high incidences are represented. The basic topology is the same for both of these cases. The separation line moves closer to the trailing edge as the angle increases, and the

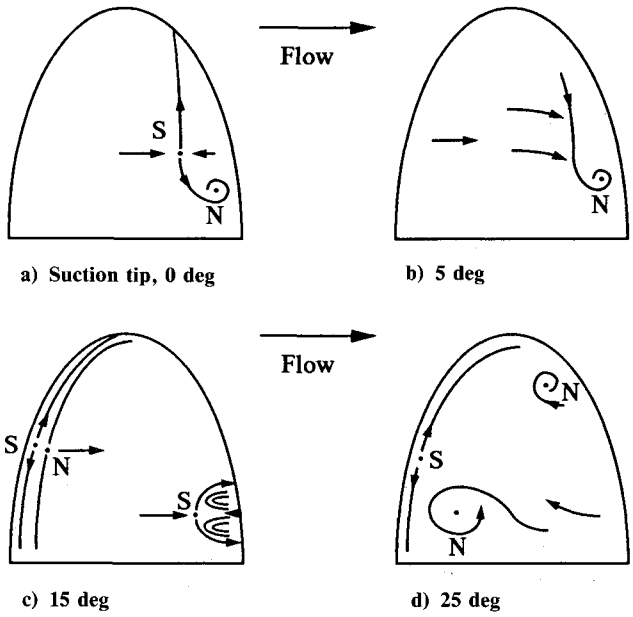

a) Suction tip, 0 deg b) 5 deg

c) 15 deg d) 25 deg

Fig. 19 Evolution of suction side topology.

reversed flow downstream of the separations emanates from a node of attachment close to or on the trailing edge.

The evolution process on the suction side is much more dramatic. Figure 19 shows the skeletal topologies for the suction surfaces at the same four angles of attack. In Fig. 19a, a separation takes place at roughly 75% chord, which rolls up into a node near the base of the wing. The tip end of the separation line does not turn upstream because the suction tip generates a pressure gradient that tends to push the flow away from the tip. This effect is even more pronounced in Fig. 19b, where the spanwise pressure gradient pushes all of the flow toward the root, eliminating the saddle point on the separation line. At a higher angle of attack, Fig. 19c, the separation takes place along the leading edge. This separation causes turbulent transition and consequently reattachment, producing a separation bubble along the leading edge. The now turbulent attached flow does not separate at 75% chord, but instead delays and constricts the separation to a small scallop-shaped region on the lower half of the wing. Delaying separation bends the separation line over into this scallop, or crescent shape, and produces two lobes of reversed flow. In Fig. 19d, the angle is increased high enough that after separation from the leading edge, the flow is unable to reattach. This allows the small scallop-shaped separation to move forward and engulf the entire suction side of the wing. Meanwhile, the two lobes of reverse flow grow to become the two large nodes shown in the figure.

IV. Concluding Remarks

Flow visualization experiments have been used to reveal the skin-friction vector field of a surface mounted semi-ellipsoidal wing. The complexity of the problem has been reduced by presenting the field in topological terms. The three major changes in the topology of the skin-friction pattern as the angle of attack was increased from 0 to 25 deg were found to result from three-dimensional pressure gradient and turbulent transition effects. As a general model for studying three-dimensional separated flows, the surface mounted semi-ellipsoid is ideal. The number of varied features revealed by this study shows that this geometry contains all the complex physics that makes these flows so interesting while retaining geometrical and mathematical simplicity. Although the experimental techniques used in this study were able to provide a very good overall picture, they were not able to precisely resolve all of the important details of the topology. Obviously, more work needs to be done, particularly in the separated flow regions and in qualifying the flow behavior across the tip of the wing. This work may require quantitative extensions into the flowfield both experimentally and numerically.

Acknowledgments

This research was supported by the Office of Naval Research, under Contract N00014-88-K-0001, Grant N00014-91-J-1204, and Grant N00014-89-J-1342 in support of the DARPA Subtech Program.

References

[1]Andronov, A. A., Leontovich, E. A., Gordon, I. I., and Maier, A. G., *Qualitative Theory of Second-Order Dynamic Systems*, Wiley, New York, 1973.

[2]Legendre, R., "Separation de L'ecoulement Laminaire Tridimensionell," *La Recherche Aeronautique*, No. 54, Nov–Dec. 1956, pp. 3–8.

[3]Lighthill, M. J., "Attachment and Separation in Three-Dimensional Flow," *Laminar Boundary Layers*, edited by L. Rosenhead, Oxford University Press, Oxford, England, UK, 1963, pp. 72–82.

[4]Wang, K. C., "Separation Patterns of Boundary Layer over an Inclined Body of Revolution," *AIAA Journal*, Vol. 10, No. 8, 1972, pp. 1044–1050.

[5]Hung, C. M., Sung, C. H., and Chen, C. L., "Computation of Saddle Point of Attachment," *AIAA Journal*, Vol. 30, No. 6, 1992, pp. 1561–1569.

[6]Hunt, J. C. R., Abell, C. J., Peterka, J. A., and Woo, H., "Kinematical Studies of the Flows Around Free or Surface-Mounted Obstacles; Applying Topology to Flow Visualization," *Journal of Fluid Mechanics*, Vol. 86, Pt. 1, 1978, pp. 179–200.

[7]Tobak, M., and Peake, D. J., "Topology of Three Dimensional Separated Flows," *Annual Review of Fluid Mechanics*, Vol. 14, 1982, pp. 61–85.

[8]Chapman, G. T., "Topological Classification of Flow Separation on Three-Dimensional Bodies," AIAA 24th Aerospaces Sciences Meeting, AIAA Paper 86-0485, Reno, NV, Jan. 1986.

[9]Maltby, R. L., and Keating, R. F. A., "The Surface Oil Flow Technique for Use in Low Speed Wing Tunnels," AGARDograph, No. 70, 1962, pp. 29–38.

[10]Parthasarathy, R. N., Sirviente, A. I., and Patel, V. C., "LDV Measurements in Separated Flow on an Elliptic Wing Mounted at an Angle of Attack on a Wall," *Separated Flows,* FED Vol. 149, edited by J. C. Dutton and L. P. Purtell, ASME Publications, New York, 1993, pp. 137–151.

[11]Johnson, T. A., "Visualization of Topology of Separated Flow Over a Semi-Elliptic Wing at Incidence Intersecting a Plane Wall," M.S. Thesis, Dept. of Mechanical Engineering, Univ. of Iowa, Iowa City, 1991.